Methods 64 (2013) 276–282

Contents lists available at ScienceDirect

Methods

journal homepage: www.elsevier.com/locate/ymeth

DNA nanostructure-based ultrasensitive electrochemical microRNA biosensor

Yanli Wen [a], Gang Liu [a,*], Hao Pei [b], Lanying Li [a], Qin Xu [a], Wen Liang [a], Yan Li [a], Li Xu [a], Suzhen Ren [a], Chunhai Fan [b,*]

[a] Division of Chemistry and Ionizing Radiation Measurement Technology, Shanghai Institute of Measurement and Testing Technology, Shanghai 201203, China
[b] Laboratory of Physical Biology, Shanghai Institute of Applied Physics, Chinese Academy of Sciences, Shanghai 201800, China

ARTICLE INFO

Article history:
Available online 2 August 2013

Keywords:
DNA nanostructure
Electrochemical DNA sensors
microRNA
Enzyme amplification

ABSTRACT

MicroRNAs (miRNAs) are key regulators of a wide range of cellular processes, and have been identified as promising cancer biomarkers due to their stable presence in serum. As an surface-based electrochemical biosensors which offer great opportunities for low-cost, point-of-care tests (POCTs) of disease-associated miRNAs. Nevertheless, the sensitivity of miRNA sensors is often limited by mass transport and the surface crowding effect at the water-electrode interface. Here, we present a protocol as well as guidelines for ultrasensitive detection of miRNA with DNA nanostructure-based electrochemical miRNA biosensor. By employing the three-dimensional DNA nanostructure-based interfacial engineering approach, we can directly detect as few as attomolar (<1000 copies) miRNAs with high single-base discrimination ability. Since this ultrasensitive electrochemical miRNA sensor (EMRS) is highly reproducible and essentially free of prior target labeling and PCR amplification, it can conveniently and reliably analyze miRNA expression levels in clinical samples from esophageal squamous cell carcinoma (ESCC) patients.

1. Introduction

There have been increasing interests in the development of rapid, sensitive, and cost-effective DNA sensing devices for sequence-specific detection of clinically, environmentally, or security-relevant nucleic acid targets. MicroRNAs (miRNAs) as promising cancer biomarkers can regulate a wide range of cellular processes at the post-transcriptional level. Since the discovery of miRNAs in Caenorhabditis elegans in 1993 [1], there has been tremendous interest in studying their pivotal roles in basic biological processes and their expression levels in various types human cancers [2].While there has been urgent need for quantitative miRNA detection both in fundamental biological studies and for diagnostic purposes, it largely remains a technical challenge due to the low abundance, short length and sequence similarity of miRNAs [3]. In recent years, many novel techniques and methods have been reported for miRNA detection, including nanopore sensors [4], fluorescent sensors [5], colorimetric sensors [6], microarray based sensor [7] and the widely used Northern blotting [8] and quantitative polymerase chain reaction (qPCR) [9,10]. Although there have been advancements with each of these methods, none of the existing methods satisfy the high standards for point-of-care testing (POCT) of miRNAs, i.e. a label-free and amplification-free method that possesses sufficiently high sensitivity and selectivity to detect very minute miRNA from serum samples, specificity to identify 1–2 mismatches within the miRNA family, and low cost and portability for applications in small clinics and/or at home.

Electrochemical sensors are well recognized to be promising point-of-care testing (POCT) device due to the ready availability of inexpensive and small-size electrochemical detectors (e.g. electrochemistry-based ubiquitous glucose meters) [11,12]. However, the sensitivity of electrochemical DNA sensors is often limited by the accessibility of target DNA/RNA molecules to probes attached to the heterogeneous electrode surface due to the reduced mass transport and the presence of surface crowding effect (in contrast to probe-target recognition in homogeneous solution) [13–16]. Hence, the sensitivity of electrochemical sensors for miRNAs (pM–fM) usually does not support direct detection of low-abundance miRNAs without prior amplification with PCR.

With the rapid emergence of DNA nanotechnology, it has been able to 'bottom-up' construct exquisite DNA nanostructures with excellent controllability and high precision arising from unmatched self-recognition properties of DNA molecules [17,18]. Our previous studies have demonstrated that a three-dimensional (3D) DNA tetrahedron-structured probe (TSP) modified with sulfur at three vertices can be rapidly and firmly adsorbed at gold surfaces [19], resulting in a nanoengineered interface which can improve the ability of biomolecular sensing [19,20]. The nanoengineered interface could provide a convenient solution to spatial

* Corresponding authors.
E-mail address: fchh@sinap.ac.cn (C. Fan).

1046-2023/$ - see front matter © 2013 Elsevier Inc. All rights reserved.
http://dx.doi.org/10.1016/j.ymeth.2013.07.035

control and enhanced accessibility of probes on the surface without relying on advanced micro/nano-fabrication technologies.

Here we exploit this DNA nanostructure-based interfacial engineering strategy and the base stacking-based strategy for short-sequence miRNAs detection. We employed the base-stacking strategy to overcome the problem of "sandwich-type" based electrochemical miRNAs (short length and low melting temperature) assays and developed an a label-free and PCR-free electrochemical miRNA sensor (EMRS) for ultrasensitive detection of attomolar miRNAs with extraordinarily high sequence specificity.

2. Materials and methods

2.1. Materials

2.1.1. Reagents

Oligonucleotides (Table 1; Invitrogen Inc.)
Synthesized mature miRNAs (Table 2; Invitrogen Inc.)
Total RNAs from tissue in three human organs (liver, prostate and lung; Ambion)
Total RNA samples from esophageal squamous cell carcinoma (ESCC) patients (provided by Zhongshan Hospital of Shanghai)
TMB substrate (TMB = 3, 3′, 5, 5′ tetramethylbenzidine; K-blue low activity substrate; Neogen)
Horseradish peroxidase-conjugated avidin (avidin-HRP; Roche Diagnostics)
Streptavidin-poly-HRP80 (poly-HRP80; Fitzgerald Industries International Inc.)
poly-HRP diluent (Fitzgerald Industries International Inc.)
Ethylene glycol-terminated thiol (HS-$(CH_2)_{11}$-EG_2-OH, OEG; Prochimia)
Diethyl pyrocarbonate, >97% (DEPC; Sigma) **!CAUTION** DEPC is hazardous of skin contact, eye contact and inhalation, which is irritant to skin, eyes and respiratory.
Tris (2-carboxyethyl) phosphine hydrochloride (TCEP; Sigma)
Tris-(hydroxymethyl)aminomethane (Tris base; Cxbio Biotechnology Ltd.)
Sulfuric acid, >98% (H_2SO_4; Sinopharm Chemical Reagent Co., Ltd.) **!CAUTION** H_2SO_4 is dangerously corrosive and can cause severe burns.
Ethylenediaminetetraacetic acid (EDTA; Sigma)
Sodium phosphate monobasic, >99% (NaH_2PO4; Sinopharm Chemical Reagent Co., Ltd.)
Sodium phosphate dibasic dodecahydrate, >99% ($Na_2HPO_4 \cdot 12H_2O$; Sinopharm Chemical Reagent Co., Ltd.)
Potassium phosphate dibasic, >99% (KH_2PO_4; Sinopharm Chemical Reagent Co., Ltd.)
Sodium chloride, >99.5% (NaCl; Sinopharm Chemical Reagent Co., Ltd.)
Potassium chloride, >99.8% (KCl; Sinopharm Chemical Reagent Co., Ltd.)
Magnesium chloride, >99.5% ($MgCl_2$; Sinopharm Chemical Reagent Co., Ltd.)
Ethanol (Sinopharm Chemical Reagent Co., Ltd.)
Milli-Q water (18 MΩ cm; Millipore)

Table 2
Sequences of mature human miRNAs.

miRBase ID	Sequence (5′–3′)	Accession#
hsa-mirR-21	UAGCUUAUCAGACUGAUGUUGA	MIMAT0000076
hsa-miR-31	AGGCAAGAUGCUGGCAUAGCU	MIMAT0000089
hsa-let-7a	UGAGGUAGUAGGUUGUAUAGUU	MIMAT0000062
hsa-let-7b	UGAGGUAGUAGGUUGUGUGGUU	MIMAT0000063
hsa-let-7c	UGAGGUAGUAGGUUGUAUGGUU	MIMAT0000064
hsa-let-7d	AGAGGUAGUAGGUUGCAUAGUU	MIMAT0000065
hsa-let-7e	UGAGGUAGGAGGUUGUAUAGUU	MIMAT0000066
hsa-let-7f	UGAGGUAGUAGAUUGUAUAGUU	MIMAT0000067
hsa-let-7g	UGAGGUAGUAGUUUGUACAGUU	MIMAT0000414
hsa-let-7i	UGAGGUAGUAGUUUGUGCUGUU	MIMAT0000415
hsa-miR-98	UGAGGUAGUAAGUUGUAUUGUU	MIMAT0000096

2.1.2. Equipments

CHI630b electrochemical workstation (CH Instruments Inc.)
CHI101 2-mm-diameter Gold working electrode (CH Instruments Inc.)
CHI115 platinum wire counter-electrode (CH Instruments Inc.)
CHI111 Ag/AgCl reference electrode (CH Instruments Inc.)
CHI220 cell stand with Φ25 mm × 40 mm glass cell (CH Instruments Inc.)
Alpha alumina powder, 0.3 mm (CH Instruments Inc.)
Gamma alumina powder, 0.05 mm (CH Instruments Inc.)
Microcloth (CH Instruments Inc.)
Himac CF16RX versatile compact centrifuge, with a model T15A34 rotor (Hitachi Koki Co., Ltd.)
U-3010 spectrophotometer (Hitachi High-Technologies Corporation)
KQ218 ultrasonic cleaning (Kunshan Ultrasonic Instruments Co., Ltd.)
Milli-Q synthesis A10 (Millipore Inc.)
Thermomixer comfort (Eppendorf Inc.)
IKA lab dancer (IKA Inc.)
HD-850 Horizontal air flow clean bench (Shanghai sujing Industrial Co., Ltd.)
PCR Peltier thermal cycler PTC-200 (MJ. Research Inc.)

2.1.3. Reagent setup

All solutions were prepared with RNase-free water. The RNase-free water was prepared with Milli-Q water (18 MΩ cm resistivity) treated with 0.1% DEPC.

Table 1
Synthetic oligonucleotide probes.

Probe name	Sequence (5′–3′)
tetra-miR-21	ACATTCCTAAGTCTGAAACATTACAGCTTGCTACACGAGAAGAGCCGCCATAGTAAAAAAAAAAATCAACATCAG
tetra-let-7d	ACATTCCTAAGTCTGAAACATTACAGCTTGCTACACGAGAAGAGCCGCCATAGTAAAAAAAAAAAAACTATGCAA
tetra-miR-31	CATCTTGCCTAAAAAAAAAAACATTCCTAAGTCTGAAACATTACAGCTTGCTACACGAGAAGAGCCGCCATAGTA
tetra-B	SH-C_6TATCACCAGGCAGTTGACAGTGTAGCAAGCTGTAATAGATGCGAGGGTCCAATAC
tetra-C	SH-C_6-TCAACTGCCTGGTGATAAAACGACACTACGTGGGAATCTACTATGGCGGCTCTTC
tetra-D	SH-C_6-TTCAGACTTAGGAATGTGCTTCCCACGTAGTGTCGTTTGTATTGGACCCTCGCAT
swRP-miR-21	TCTGATAAGCTA-BIOTIN′
swRP-let-7d	CCTACTACCTCT-BIOTIN′
swRP-miR-31	BIOTIN′-AGCTATGCCAG
SH-ss-miR-21	SH-C_6-TAAATAAATATCAACATCAG
miD-21	TAGCTTATCAGACTGATGTTGA

Phosphate buffer (PB) 10 mM Na_2HPO_4/$NaH2PO_4$ (pH 7.4)
Phosphate buffer saline (1 × PBS) 10 mM Na_2HPO_4 + 2 mM KH_2PO_4 + 37 mM NaCl + 2.7 mM KCl (pH 7.4).
Imobilization buffer (TM-buffer) 20 mM Tris + 50 mM $MgCl_2$ (pH 8.0)
Hybridization buffer (H-buffer) 10 mM PB + 1 M NaCl + 20 mM $MgCl_2$
Electrochemistry buffer (E-buffer) The K-blue low activity TMB substrate in the format of a ready-to-use reagent
Washing buffer (W-buffer) 1 × PBS
TE buffer 10 mM Tris + 1 mM EDTA (pH 8.0)
TCEP solution 30 mM in water (pH7.0)

2.1.4. Equipment setup

Setup of the horizontal air flow clean bench A horizontal air flow clean bench is placed in a RNase-free room, and a standard sterilized process was carried out before the experiment.

Setup of the electrochemical cell A conventional three-electrode system is used in the experiment, with a gold working electrode, a platinum wire auxiliary electrode and an Ag/AgCl reference electrode. A glass electrochemical cell is placed on the cell stand, plugged with three electrodes. 1 mL E-buffer is added to the cell.

2.2. Design for electrochemical miRNAs sensor

In this design, a capture DNA probe (probe1, 10 bases) appended to one vertex of the tetrahedron-structured probe (TSP) is complementary to part of the target miRNAs (22 bases). The TSP also contains three thiol groups at the other three vertices for its immobilization at the Au surface. A biotin-tagged DNA strand (probe 2, 12 bases) serves as the signal probe, which is complementary to the miRNA sequence adjacent to that matches the probe 1. Hence, the three parts are held into a sandwich structure by both the base pairing between the probes and the miRNA target and the base stacking forces between the padlock probes [7]. The biotin tag at the end of the signal probe 2 can specifically bind to avidin-HRP or poly-HRP80, which catalyze the reduction of hydrogen peroxide and generate quantitative electrochemical current signals in the presence of the co-substrate, 3, 3′, 5, 5′ tetramethylbenzidine (TMB) (shown in Fig. 1).

2.3. The preparation of DNA nanostructure capture probes

Tetrahedral nanostructure-based capture probes for miRNA detection (Tetra-miR-21) were formed as the following steps:

1. Four strands, tetra-miR-21, tetra-B, tetra-C and tetra-D were dissolved in TE buffer yielding a final concentration of 50 μM. **CRITICAL STEP** make sure the concentration of four strands exactly equivalent.
2. Add 1 μL of 50 μM tetra-miR-21, tetra-B, tetra-C and tetra-D to 41 μL of TM buffer respectively, and then add 5 μL of TCEP solution to the mixture to reduce the thiol groups and thus activate the thiolated DNA. Of note, the presence of TCEP does not interfere with the assembly, thus the cleaved DNA is not purified.
3. The resulting mixture was heated to 95 °C for 2 min, then cooled to 4 °C over 30 s using a Peltier thermal cycler PTC-200, after that, the Tetra-miR-21 DNA nanostructure was formed.

? TROUBLESHOOTING

Similarly, the self-assembly of the Tetra-let-7d and Tetra-miR-31 DNA nanostructures were same as the Tetra-miR-21, just changed the tetra-miR-21 probe with tetra-let-7d and tetra-miR-31 probes.

2.4. The gold working electrode assemble process

1. Gold electrodes were cleaned following the reported protocol [11]. **CRITICAL STEP** it is essential to make a clean gold surface and avoid deposition of contaminants on the metal surface, the cleaned electrodes should be immediately used for DNA immobilization.
2. 3 μL of 1 μM tetrahedral nanostructure-based capture probes (Tetra-miR-21 probes) were pipetted to the cleaned gold electrode, same as the Tetra-let-7d and Tetra-miR-31 probes.
3. Cap the electrodes with plastic electrode caps and incubate overnight at room temperature. **CRITICAL STEP** all the electrodes should be well capped to prevent solutions at the top of them from drying up. If the environmental humidity is too low, the use of a humidistat is recommended.
4. Rinse the electrodes with 1 × PBS and blow-dry the electrodes with nitrogen before hybridization.

2.5. Hybridization of miRNA with capture probes modified electrodes

1. Add 10 μL of complementary miRNA or cognate miRNA or non-cognate miRNA or total RNAs from human tissues in appropriate concentrations (a series of concentrations ranging from attomolar to nanomolar) and 10 μL of 5 μM biotinylated reporter probe in a 2 mL RNase-free centrifuge tube containing 80 μL hybridization buffer.
2. Mix the above solution and heat to 80 °C for 5 min, then cool the mixture to room temperature more than 20 min.

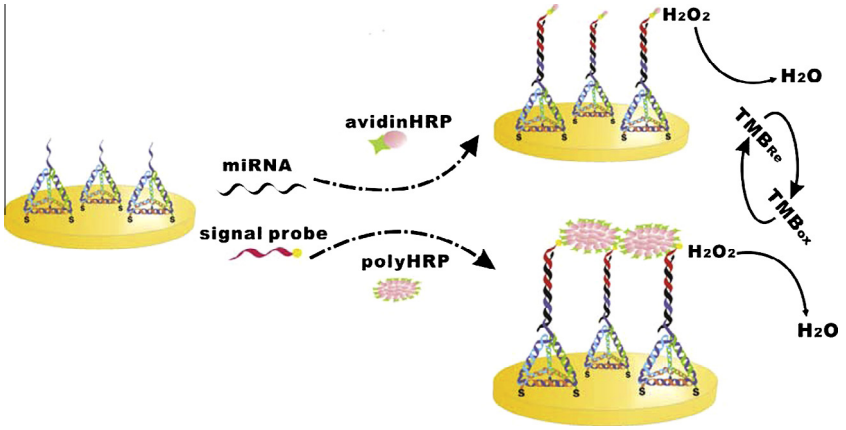

Fig. 1. Scheme for miRNA detection with the tetrahedron-based electrochemical miRNAs sensor (EMRS) with enzyme-based signal transduction (either avidin-HRP or high-activity poly-HRP80). (Adapted from Ref. [21])

3. Dip the tetrahedral nanostructure-based gold electrode or thiolated single-stranded DNA modified gold electrode into the centrifuge tube and incubate at 10 °C for 5 h. **CRITICAL STEP** the hybridization time and temperature are very important for the hybridization efficiency, the optimal conditions can generate the optimal signal noise ratio (as shown in Fig. 2).
   ? TROUBLESHOOTING
4. Rinse the hybridized electrode with 1 × PBS stored in 4 °C refrigerator and blow-dry with nitrogen. **CRITICAL STEP** the cooled washing buffer is essential for the hybridized DNA/RNA, which can reduce the melting of double strand DNA/RNA.
5. Add 3 μL of avidin-HRP (0.5 U/mL) or poly-HRP80 (1 μg/mL) to the surface of the electrode, cap the electrode with plastic electrode caps and incubate for 15 min at 4 °C refrigerator. **CRITICAL STEP** the enzymatic activity of HRP effect the stability of detection signal, so keep the stable activity of enzyme is very important.
   ? TROUBLESHOOTING
6. Rinse the electrode with 1 × PBS stored in 4 °C refrigerator, wipe off the buffer of the electrode except the surface of gold, cap the electrode with plastic electrode caps and then subject to electrochemical measurements.

2.6. Electrochemical measurements

1. Place a glass electrochemical cell on the cell strand, add 1 mL E-buffer to the cell, plug a platinum wire auxiliary electrode, an Ag/AgCl reference electrode and the gold working electrode to the cell and connect the three electrodes to the CHI 630 electrochemical workstation.
2. Carry out the cyclic voltammetry (CV) to scan the working electrode with a scan rate of 100 mV/s, the potential ranged from 0 to 0.7 V. The CV curves exhibit typical redox peakers of TMB (shown in Fig. 3A).
3. Carry out the amperometry to detect the electrocatalytic reduction current of the electrode, the potential fixed at 100 mV and the signal current was measured at 100 s after the HRP redox reaction reached steady state (shown in Fig. 3B).

? TROUBLESHOOTING

2.7. Troubleshooting guide

Trouble shooting advice in Table 3.

3. Results and discussions

3.1. Electrochemical behavior of EMRS

Fig. 3A displays cyclic voltammograms (CVs) of the HRP-based electrocatalytic process of EMRS for the detection of a cancer-associated has-miR-21 microRNA (miR-21). When miR-21 was absent, we observed two pairs of well-defined redox peaks that were assigned to the two-electron reduction and oxidation reactions of TMB, suggesting that the presence of the tetrahedral nanostructure did not significantly interfere with the electron communication between TMB and the underlying gold electrode [22]. This indicates that while the monolayer is relatively thick (~6 nm as estimated from the duplex length), it is still amenable to electrochemical transduction with enzymatic amplification due to the fact that tetrahedra are hollow structures. This unique property makes it particularly useful for the development of high-sensitivity miRNAs

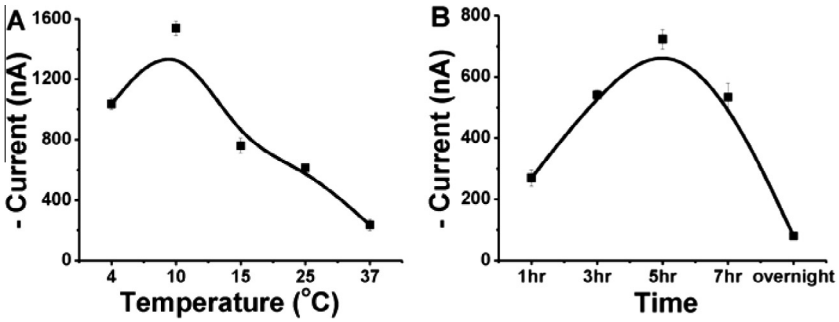

Fig. 2. Effect of (A) hybridization tempareture (of 1 nM miR-21 in 5 h hybridization) and (B) hybridization time (of 10 pM miR-21 hybridization at 10 °C) for tetrahedra-based EMRS. Error bars represent standard deviations for measurements taken from at least three independent experiments [21].

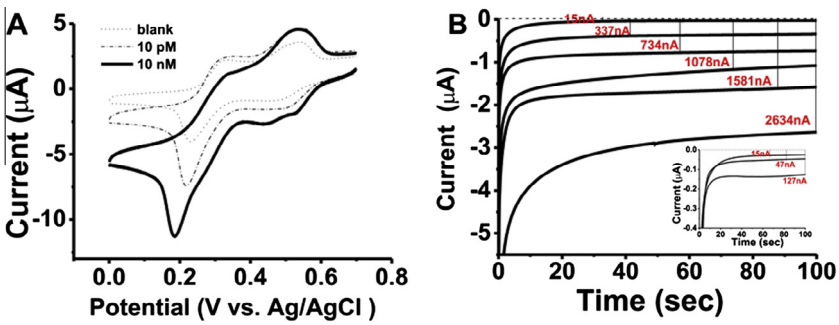

Fig. 3. (A) Cyclic voltammograms for EMRS in the absence (- - -) and presence of 10 pM (-·-·-) and 10 nM miR-21(—). Scan rate: 100 mV/s. (B) Amperometric curves (*i*-*t*) for EMRS tested with a series of miR-21 concentrations. From top to bottom: 0 pM, 1 pM, 10 pM, 100 pM, 1 nM, 10 nM. Insert shows the low concentration range of the *i*-*t* curves for 10 fM and100 fM miR-21. The potential was held at 100 mV [21].

Table 3
Troubleshooting table.

Step	Problem	Cause	Solution
2.3 Step3	Tetrahedron formed with low efficiency	Nonequivalent concentration of four DNA strands	Quantify the DNA concentration precisely by UV spectrophotometer
2.5 Step3	Temperature control is not accurate	Low temperature is difficult to controlled by ordinary water bath in hot day	Use a thermostat with cool function
2.5 Step 5	Unstable enzyme activity	Unstable dilution solvent	Choose the specialized poly-HRP diluent to keep the stability of enzyme
2.6 Step 3	Week or no signal	Tetrahedron is not immobilized onto the gold surface	Clean the gold electrode surface and use freshly prepared tetrahedron

sensors since it reduces the surface effect (increased layer thickness) without sacrificing electrochemical reactivity.

In the presence of miR-21, we found that the reduction peak located at ~200 mV apparently increased, leading to a pair of asymmetric redox peaks that was characteristic of the occurrence of electrocatalysis. This implied that miR-21 was captured onto the TSP surface and formed a "sandwich" structure with the biotinylated reporter DNA, leading to the binding of avidin–HRP to the biotinylated DNA signal strands and subsequently the localization of the HRP enzyme to the electrode surface. Here, TMB served as an electron shuttle that could diffuse in and out of the redox site of the HRP, which coupled the catalytic reduction of H_2O_2 to the electrode surface and resulted in the observed electrocatalytic peaks. Amperometry provides a direct way to characterize this HRP-catalyzed electrochemical process. Upon the onset of the potential at 100 mV, we instantly observed a decay curve for current (I) versus time (t), which reached a plateau (steady-state current) within ~100 s (Fig. 3B). The background current of EMRS was as low as ~15 nA, suggesting the presence of minimal non-specific binding (NSB) of either DNA strands or the enzyme. Significantly, the signal-to-background ratio approached nearly 200 when the target concentration was 10 nM [21]. We then challenged the EMRS with a series of concentrations of the synthetic miR-21 target in the range from 10 fM to 10 nM. The amperometric signal increased monotonically with the logarithm concentration of miR-21, resulting in a typical dose–response curve (Fig. 4). The detection limit of EMRS was determined to be 10 fM as the electrochemical signal for 10 fM miR-21 was still significantly larger than the background (.3 SD; Fig. 4, inset).

3.2. Sensitivity and specificity of EMRS

To further improve the sensitivity, we employed poly-HRP80, a polymerized streptavidin-HRP conjugate with up to 400 HRP molecules per conjugate. While poly-HRP80 is of high catalytic activity, it often increases the background as well due to significant non-specific adsorption. Given the high protein resistance ability of DNA nanostructure-decorated surfaces, we expected that poly-HRP80 could amplify the electrochemical signal without increasing the background current. Indeed, we found that the background almost remained the same while the signal was greatly enhanced (Figs. 4 and 5A). The EMRS signal for 10 fM with avidin-HRP had become indistinguishable with the background, however the poly-HRP80-based EMRS could detect as few as 10 aM miRNAs (600 molecules in 100 μL), which represented a sensitivity improvement by three orders of magnitude. Moreover, poly-HRP80-based EMRS had an extremely large dynamic range, covering nine orders of magnitude.

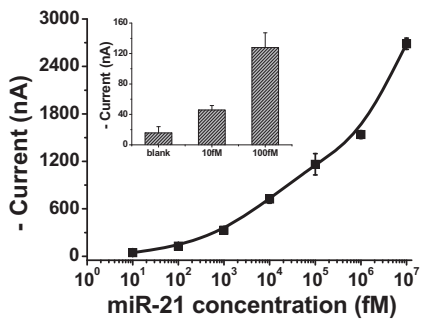

Fig. 4. Logarithmic plot of amperometric current vs miR-21 concentration for EMRS. Error bars represent standard deviations for measurements taken from at least three independent experiments [21].

We then tested the specificity of EMRS by using a family of human let-7 sequences of 1 pM possessing closely related sequences with high homology (variation by only 1–3 nt) [23]. Importantly, we found that EMRS with the designed probe for let-7d led to significantly higher (by at least 3-fold) electrochemical signal for let-7d than other let-7 miRNAs and non-cognate sequences ($P < 0.05$) (Fig. 5B). In fact, with the exception of let-7a and let-7e containing G/T substitutions that have relatively high binding energy [24,25], the signals for all other let-7 sequences were at least 1–2 orders of magnitude lower than that for let-7d. This high mismatch discrimination ability reflects the high specificity offered by the nanostructured probes at the surface.

EMRS could also differentiate precursor miRNAs (pre-miRNAs) from mature ones. Pre-miRNAs are spliced in vivo to form mature miRNAs that can be assembled into active RNA-induced silencing complexes (RISCs) [26], hence their co-existence often results in false-positives [27]. EMRS was challenged with a hairpin-structured precursor human miRNA, pre-miR-31 [28], and mature miR-31 sequences. Significantly, the signal for the precursor was nearly 2 orders of magnitude lower than that for mature miR-31 (Fig. 5C), indicating that EMRS could effectively suppress the signal for pre-miRNAs and realize error-free detection of miRNAs.

The 3D DNA nanostructure-based EMRS thus provides an ultrasensitive approach for reliable quantitative detection of attomolar miRNAs with extraordinarily high sequence specificity. Compared to previously reported electrochemical DNA sensors, EMRS shows several combined advantages. First, DNA probes are uniformly distributed on spatially isolated DNA tetrahedral nanostructures that minimize inter-strand interactions and facilitate hybridization. Also, the relatively large nanostructure places the probes 6 nm over the Au surface, making them stay in a solution-like environment [19]. Second, DNA tetrahedra-modified surfaces are inherently proteinresistant [19], which greatly minimizes the background and allows high signal amplification with poly-HRP80 without sacrificing the signalto-background ratio. Third, the very rigid structure of DNA tetrahedral and the presence of three thiols per nanostructure result in highly stable and reproducible self-assembled nanostructure surfaces, contributing to both the low background and small electrode-to-electrode variation. Finally, given that EMRS is based on normal Au surfaces, it is fully compatible with the low-cost screen printed electrode technology

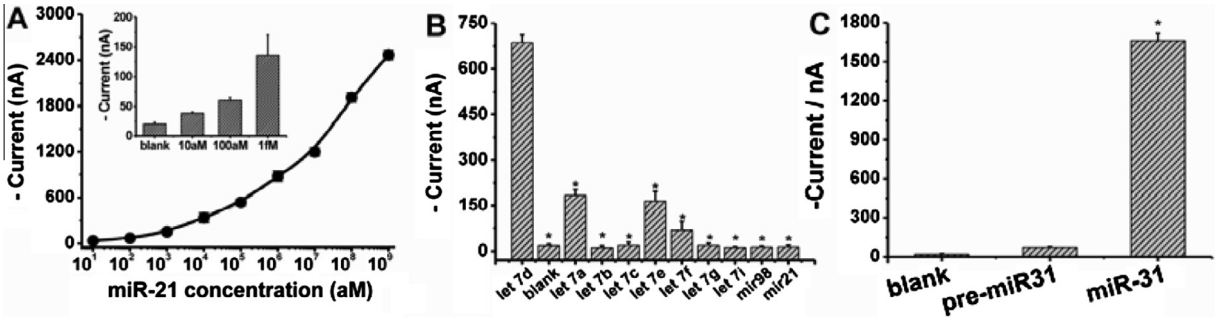

Fig. 5. Sensitivity and specificity of the tetrahedra-based EMRS with poly-HRP80 amplification. (A) Logarithmic plot of amperometric current vs miR-21 concentration for tetrahedra-based EMRS with poly-HRP amplification. Insert shows the low concentration range of miR-21. (B) Discrimination of let 7 family members, miR-21 used as negative control (all of 1 pM), $^{*}P < 0.05$ significantly different from the let-7d, and (C) Pre/mature-miRNA discrimination (of 10 pM), $^{*}P < 0.05$ significantly different from the pre-miR-31 and blank. Error bars represent standard deviations for measurements taken from at least three independent experiments [21].

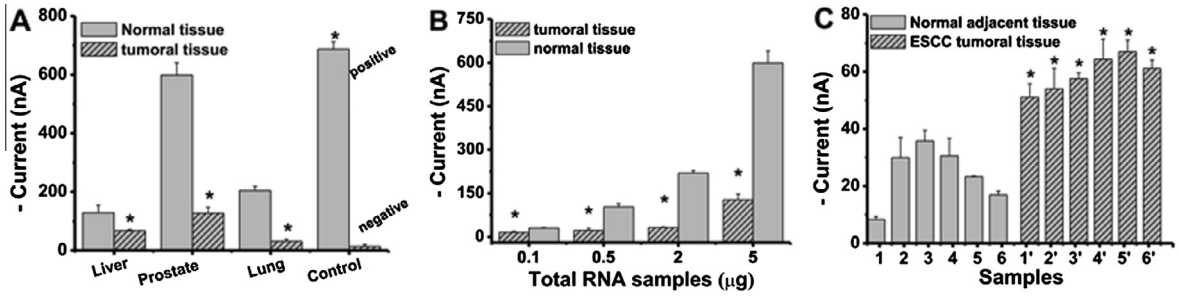

Fig. 6. (A) Signals of EMRS for let-7d in total RNAs (5.0 μg) extracted from liver, lung and prostate tissues. Synthetic let-7d (1 pM) was used as positive control and the negative control was the signal obtained in the absence of total RNAs. (B) Detection of let-7d with EMRS using different amount of total RNAs from prostate tumoral tissue and normal tissue. (C) Detection of miR-21 with EMRS in the total RNA of esophageal squamous cell carcinoma (ESCC) patients (all of 100 ng). Statistical analysis was performed by paired *t*-test. $^{*}P < 0.05$ significantly different from relative normal tissue. Error bars represent standard deviations for measurements taken from at least three independent experiments [21].

and easily scalable for mass production of sensors. When coupled with portable electrochemical detectors, EMRS can provide a solution to directly detecting miRNA biomarkers in the POCT setting, which is otherwise difficult with qPCR or other solution-phase amplification methods.

3.3. Application of EMRS in real patient samples

Given the ultrahigh sensitivity and excellent sequence specificity of our tetrahedra-based EMRS, we attempted to analyze expression levels of hsa-let-7d miRNA in total RNAs extracted from tumoral and normal tissues of human liver, lung and prostate. We found that the expression levels of hsa-let-7d in tumoral tissues were significantly lower than that detected in normal tissues ($P < 0.05$; Fig. 6A), suggesting downregulated expression of hsa-let-7d in tumoral tissues that correlates well with the previous reported literature [23,26]. We further found that 100 ng of total RNA was sufficient for EMRS-based profiling (Fig. 6B). We next challenged EMRS for detection of miR-21 in clinical samples of esophageal squamous cell carcinoma (ESCC). Total RNAs (100 ng) were extracted from esophageal tumoral tissue and adjacent normal tissues collected from six ESCC patients. Fig. 6C shows that the miR-21 expressional levels in the ESCC tumoral tissues were systematically higher than those in adjacent normal tissues, suggesting an up-regulation of miR-21 expression in the tumoral tissue. Collectively, the mean level of miR-21 was increased by a factor of 2.5 in the esophageal tumor tissues compared with the adjacent normal tissues as measured by EMRS ($P < 0.05$), which was similar to the literature value of 2–4-fold change in ESCC tumoral tissue versus normal tissues [29,30].

4. Conclusions

In this report, we described the protocol of DNA nanostructure-based interface engineering for electrochemical miRNAs assays and employed the EMRS for ultrasensitive detection of miRNAs with poly-HRP enzyme amplification. while detection abilities of bioassays are often hampered in real, complex biological samples, EMRS has demonstrated excellent real applicability by its performance in analysis of clinical samples. Therefore, we expect that this highly sensitive and inexpensive DNA nanotechnology-based EMRS will become a promising miRNA quantification method in clinical diagnostics.

Acknowledgment

This work was supported by National Science Foundation of China (NSFC 21205079,21305091) and Shanghai Municipal Science and Technology Commission (12ZR1448300).

References

[1] R.C. Lee, R.L. Feinbaum, V. Ambros, Cell 75 (1993) 843–854.
[2] A. Esquela-Kerscher, F.J. Slack, Nat. Rev. Cancer 6 (2006) 259–269.
[3] K.A. Cissell, S. Shrestha, S.K. Deo, Anal. Chem. 79 (2007) 4754–4761.
[4] B.M. Venkatesan, R. Bashir, Nat. Nanotechnol. 6 (2011) 615–624.
[5] B.C. Yin, Y.Q. Liu, B.C. Ye, J. Am. Chem. Soc. 134 (2012) 5064–5067.
[6] U.H. Yildiz, P. Alagappan, B. Liedberg, Anal. Chem. 85 (2012) 820–824.
[7] D. Duan, Nucleic Acids Res. 39 (2011) e154.
[8] É. Várallyay, J. Burgyán, Z. Havelda, Methods 43 (2007) 140–145.
[9] C. Chen, D.A. Ridzon, A.J. Broomer, Z. Zhou, D.H. Lee, J.T. Nguyen, M. Barbisin, N.L. Xu, V.R. Mahuvakar, M.R. Andersen, Nucleic Acids Res. 33 (2005) e179.
[10] Z. Yu, Y. Zhu, Y. Zhang, J. Li, Q. Fang, J. Xi, B. Yao, Talanta 85 (2011) 1760–1765.
[11] J. Zhang, S.P. Song, L.H. Wang, D. Pan, C.H. Fan, Nat. Protoc. 2 (2007) 2888–2895.

[12] Y. Xiang, Y. Lu, Nat. Chem. 3 (2011) 697–703.
[13] P. Gong, R. Levicky, Proc. Natl. Acad. Sci. 105 (2008) 5301–5306.
[14] T.M. Squires, R.J. Messinger, S.R. Manalis, Nat. Biotechnol. 26 (2008) 417–426.
[15] L. Soleymani, Z.C. Fang, E.H. Sargent, S.O. Kelley, Nat. Nanotechnol. 4 (2009) 844–848.
[16] H. Yang, A. Hui, G. Pampalakis, L. Soleymani, F.F. Liu, E.H. Sargent, S.O. Kelley, Angew. Chem. Int. Ed. 48 (2009) 8461–8464.
[17] N. Seeman, Nature 421 (2003) 427–431.
[18] H. Yan, Science 306 (2004) 2048–2049.
[19] H. Pei, N. Lu, Y. Wen, S. Song, Y. Liu, H. Yan, C. Fan, Adv. Mater. 22 (2010) 4754–4758.
[20] N. Mitchell, R. Schlapak, M. Kastner, D. Armitage, W. Chrzanowski, J. Riener, P. Hinterdorfer, A. Ebner, S. Howorka, Angew. Chem. Int. Ed. 48 (2009) 525–527.
[21] Y. Wen, H. Pei, Y. Shen, J. Xi, M. Lin, N. Lu, X. Shen, J. Li, C. Fan, Sci. Rep. 2 (2012) 867.
[22] Y. Wen, H. Pei, Y. Wan, Y. Su, Q. Huang, S. Song, C. Fan, Anal. Chem. 83 (2011) 7418–7423.
[23] S. Roush, F.J. Slack, Trends Cell Biol. 18 (2008) 505–516.
[24] I. Lee, S.S. Ajay, H. Chen, A. Maruyama, N. Wang, M.G. McInnis, B.D. Athey, Nucleic Acids Res. 36 (2008) e27.
[25] L.A. Neely, S. Patel, J. Garver, M. Gallo, M. Hackett, S. McLaughlin, M. Nadel, J. Harris, S. Gullans, J. Rooke, Nat. Methods 3 (2006) 41.
[26] A. Esquela-Kerscher, F.J. Slack, Cancer 6 (2006) 259–269.
[27] D. Duan, K. Zheng, Y. Shen, R. Cao, L. Jiang, Z. Lu, X. Yan, J. Li, Nucleic Acids Res. 39 (2011) e154.
[28] E. Lund, S. Guttinger, A. Calado, J.E. Dahlberg, U. Kutay, Science 303 (2004) 95–98.
[29] R. Ogawa, H. Ishiguro, Y. Kuwabara, M. Kimura, A. Mitsui, T. Katada, K. Harata, T. Tanaka, Y. Fujii, Med. Mol. Morphol. 42 (2009) 102–109.
[30] A. Feber, L. Xi, J.D. Luketich, A. Pennathur, R.J. Landreneau, M. Wu, S.J. Swanson, T.E. Godfrey, V.R. Litle, J. Thorac. Cardiovasc. Surg. 135 (2008) 255–260.